

Dark Dwarfs: Dark Matter-Powered Sub-Stellar Objects Awaiting Discovery at the Galactic Center

Djuna Croon,^{1,*} Jeremy Sakstein,^{2,†} Juri Smirnov,^{3,‡} and Jack Streeter¹

¹*Institute for Particle Physics Phenomenology, Department of Physics, Durham University, Durham DH1 3LE, U.K.*

²*Department of Physics & Astronomy, University of Hawai'i,*

Watanabe Hall, 2505 Correa Road, Honolulu, HI, 96822, USA

³*Department of Mathematical Sciences, University of Liverpool, Liverpool, L69 7ZL, United Kingdom*

(Dated: August 5, 2024)

We investigate the effects of dark matter annihilation on objects with masses close to the sub-stellar limit, finding that the minimum mass for stable hydrogen burning is larger than the $\sim 0.075M_{\odot}$ value predicted in the Standard Model. Below this limit, cooling brown dwarfs evolve into stable dark matter-powered objects that we name *dark dwarfs*. The timescale of this transition depends on the ambient dark matter density ρ_{DM} and circular velocity v_{DM} but is independent of the dark matter mass. We predict a population of dark dwarfs close to the galactic center, where the dark matter density is expected to be $\rho_{\text{DM}} \gtrsim 10^3 \text{ GeV/cm}^3$. At larger galactic radii the dark matter density is too low for these objects to have yet formed within the age of the universe. Dark dwarfs retain their initial lithium-7 in mass ranges where brown/red dwarfs would destroy it, providing a method for detecting them.

Discovering the microphysical description of dark matter (DM) is a paramount goal of particle physics and cosmology. All of our current evidence for DM's existence is indirect, and we have no information pertaining to its mass and interactions with visible matter or other dark sector particles. We do however know that DM needs to be produced in the early universe. Among the many mechanisms for this, thermal freeze-out is a well-motivated minimal scenario. Provided that Standard Model (SM) particles are present in the final states of the process that sets the relic density, there is an energy transfer to the visible sector [1–4]. This process can be detected via annihilation signals in space [5, 6], or scattering in the laboratory [7, 8], but also affects astrophysical objects [9–35].

Objects that are not supported by nuclear burning such as white dwarfs, neutron stars [36–76], planets [77–80], and brown dwarfs [74, 81] have been shown to exhibit observable signatures based on DM interactions, as an additional energy injection can lead to changes in their structure and evolution. These objects are also excellent probes of gravity [82, 83].

In this work we investigate the effects of energy injection from DM annihilation on celestial bodies at the stellar mass boundary. These objects, which have masses $M \lesssim 0.1M_{\odot}$, are too light to fuse hydrogen on the PPI chain due to their cool core temperatures $T \sim 10^6 \text{ K}$. Those heavier than $\sim 0.075M_{\odot}$, red dwarfs or M-dwarfs, evolve into equilibrium states that fuse hydrogen to helium-3. Lighter bodies, so called brown dwarfs, are unable to do so. They experience transitory periods of hydrogen, lithium, and deuterium burning, but ultimately cool and contract eternally.

* djuna.l.croon@durham.ac.uk; 0000-0003-3359-3706

† sakstein@hawaii.edu; 0000-0002-9780-0922

‡ juri.smirnov@liverpool.ac.uk; 0000-0002-3082-0929

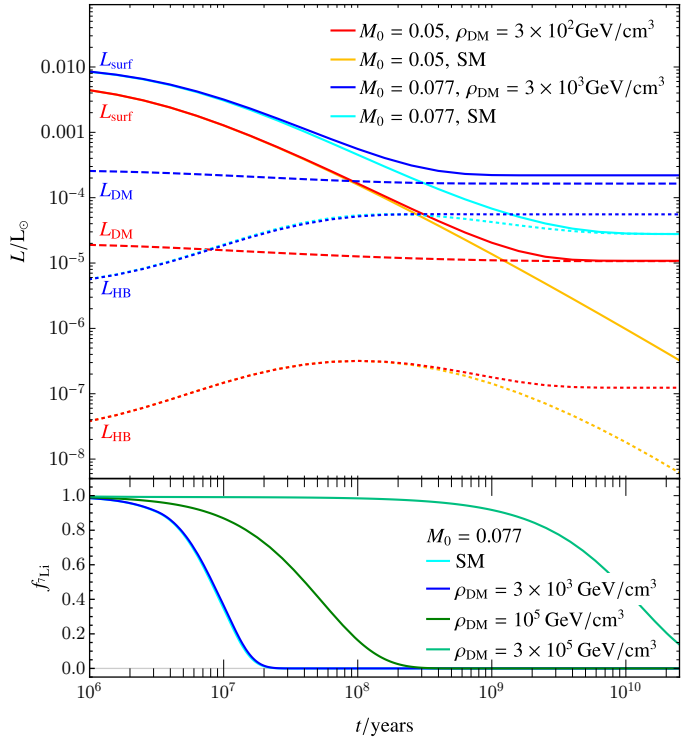


FIG. 1. Effects of DM energy injection on luminosity and lithium depletion for objects with masses $M_0 \equiv M/M_{\odot}$. **Upper panel:** time-evolution of the total luminosity L_{surf} (solid lines), luminosity from DM burning L_{DM} (dashed lines) and luminosity in hydrogen burning (dotted lines). **Lower panel:** time evolution of the surviving fraction of ${}^7\text{Li}$. Dark dwarfs retain their initial lithium-7 while red dwarfs deplete it.

As shown in Fig. 1 the situation is dramatically different when DM annihilation is present. Contracting objects attain an equilibrium configuration where they are supported primarily by DM heating. This steady-state exists for any non-zero DM density, but is attained in a Hub-

ble time for $\rho_{\text{DM}} \gtrsim 10^3 \text{ GeV cm}^{-3}$. We name these objects *Dark Dwarfs* (DDs), and differentiate them from red dwarfs near the hydrogen burning limit — $M \sim 0.075 M_{\odot}$ in the SM — which are supported by a combination of nuclear burning and DM heating. DDs are physically distinct from brown/red dwarfs in several ways:

- They are predominantly powered by DM heating, exhibiting a component of stable hydrogen burning.
- Their luminosity, radius, and effective temperature are constant in time.
- Lithium depletion occurs at larger threshold masses than the SM prediction.

These properties, which are exemplified in Fig. 1, are independent of the DM mass but do depend upon the ambient DM density and velocity dispersion. DDs can be identified by their enhanced lithium abundance despite a relatively large mass, and old stellar age.

Analytic Model for Dark Dwarfs — Sub-stellar objects are relatively simple compared with more massive bodies. Their homogeneous structure and lack of strong nuclear burning make them well-described by analytic models. They are supported by a combination of the degeneracy pressure of the electrons and the gas pressure of the ions. Under these assumptions the equation of state (EOS) is that of an $n = 3/2$ polytrope except near the surface where there is a transition to a phase of molecular hydrogen [84]. The full details of this model are reviewed in the Supplementary Material.

For our purposes, it is sufficient to begin with the model's prediction for the surface luminosity:

$$\frac{L_{\text{surf}}}{L_{\odot}} = \frac{0.0578353 b_1^3 M_0}{\kappa_R} \psi^{3\nu} \left(\frac{M_0^{5/3} \psi^{-\nu}}{b_1 \kappa_R (1 + \gamma + \alpha \psi)^2} \right)^{1/7}. \quad (1)$$

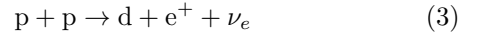
where $M_0 = M/M_{\odot}$, κ_R is the Rosseland mean opacity at the photosphere (we set $\kappa_R = 0.01 \text{ cm}^2/\text{g}$ in what follows, typical for these objects), b_1 and ν are parameters of the molecular hydrogen EOS (we shall use parameter point D in the numerical calculations in this work, defined in table S1 in the Supplemental Material, with $b_1 = 2$ and $\nu = 1.6$), $\psi = k_B T/E_F$ is the degeneracy parameter, and γ is a function of ψ given in Eq. (S4). The properties of the star are completely determined once a value of ψ is specified. The steady-state condition that determines ψ is energy conservation — the surface luminosity must balance the luminosity from all heat sources:

$$L_{\text{surf}} = \sum_i L_i \quad (2)$$

where i runs over all processes injecting energy into the star, which in our case include nuclear burning and dark matter annihilation. The polytropic approximation ceases to be valid in very low mass objects because Coulomb scattering begins to become important [85–87]. This breakdown happens for $M \lesssim 0.18 M_{\odot}$ in the SM and, as derived in Appendix ID, breaks down at lower

masses when the DM energy injection is important. The $n = 3/2$ approximation remains valid for all objects studied in this work.

Before investigating the effects of DM, it is instructive to review SM objects, which are supported solely by hydrogen burning. The central temperatures are not sufficient to fuse ^3He to ^4He so the PP-chain is only comprised of the reactions



The luminosity from these processes, assuming the $n = 3/2$ polytrope, is [84]

$$\frac{L_{\text{HB}}}{L_{\odot}} = 7.33 \times 10^{16} M_0^{11.977} \frac{\psi^{6.0316}}{(1 + \gamma(\psi) + \alpha\psi)^{16.466}}, \quad (5)$$

which was calculated by integrating the energy generation rates over the volume of the star. At the core temperatures and densities relevant for the objects we study, the majority of the thermonuclear energy is produced from deuterium burning. Imposing energy conservation, stable hydrogen burning is achieved whenever $L_{\text{HB}} = L_{\text{surf}}$, which yields

$$M_0 = 0.03362 b_1^{0.26605} \frac{(1 + \gamma(\psi) + \alpha\psi)^{1.5069}}{\psi^{0.266053\nu - 0.56165}}. \quad (6)$$

There is a minimum value of ψ for which Eq. (6) has solutions. Below this, the object cannot burn hydrogen stably because the core temperatures and densities are too low to sustain a sufficient nuclear burning rate to balance the surface luminosity. This boundary corresponds to the minimum mass for hydrogen burning (MMHB). Stars heavier than this are red dwarfs while lighter objects are brown dwarfs. In our model, the specific value is $M_{\text{MMHB}} = 0.075 M_{\odot}$, consistent with the literature e.g., [84, 87].

To calculate the effects of DM energy injection, we will work in the limit of capture-annihilation equilibrium where the amount of DM captured by the object precisely balances that lost to annihilation. This equilibrium is reached on time scales of $\sim \text{Myr}$ and shorter assuming DM annihilation rates compatible with thermal freezeout (see the appendix of Ref. [81] for a detailed discussion of this). We assume that the energy from the DM injection reaches the surface without delay. This is justified because the objects we consider are fully convective with convection time-scales of order years [88] and velocities $v_{\text{conv}} \sim 10^4 \text{ cm/s}$ (see Fig. 10 of [88]), the time to reach the surface is then ~ 100 days, far shorter than the cooling timescale of the object. Under these assumptions, the DM heat injection rate is given at any point of the stellar

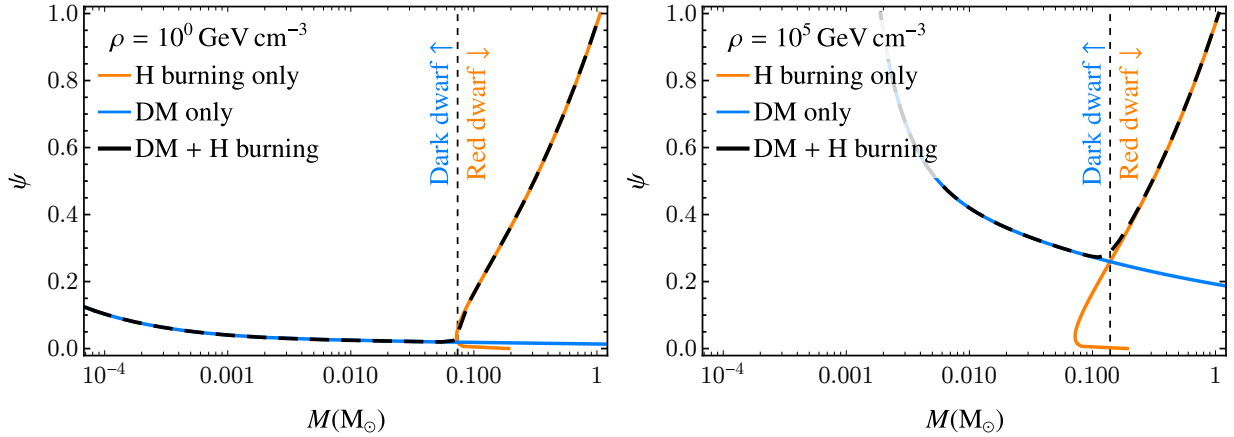


FIG. 2. Degeneracy parameter ψ as a function of mass for stars supported by both hydrogen burning and DM annihilation. The blue curves show solutions where $L_{\text{surf}} = L_{\text{DM}}$ (including gravitational focusing), corresponding to stars supported solely by DM annihilation; the orange curve shows solutions for the SM case where objects are supported solely by hydrogen burning, $L_{\text{surf}} = L_{\text{HB}}$; and the black dashed lines show the solution for the general case $L_{\text{surf}} = L_{\text{DM}} + L_{\text{HB}}$. Lighter objects are primarily DM supported (dark dwarfs) whereas heavier masses behave like SM H-burning stars (red dwarfs).

evolution by [34, 81, 89]

$$L_{\text{DM}} = m_{\text{DM}} \pi R^2 \Phi, \quad \text{with} \\ \Phi = \sqrt{\frac{8}{3\pi} \frac{\rho_{\text{DM}} v_{\text{DM}} f_{\text{cap}}}{m_{\text{DM}}}} \left(1 + \frac{3}{2} \frac{v_{\text{esc}}^2}{v_{\text{DM}}^2} \right) \quad (7)$$

where $v_{\text{esc}}^2 = 2GM/R$ is the escape velocity, ρ_{DM} is the ambient DM density, v_{DM} is circular velocity of galactic DM, f_{cap} is the fraction of DM captured that we set to unity, and m_{DM} is the DM mass; the term in the brackets accounts for gravitational focusing. Throughout this work, we fix $v_{\text{DM}} = 50$ km/s as a conservative benchmark [90]. These equations have an important consequence: the DM luminosity is independent of the DM mass. Since the properties of the object are determined solely by energy conservation, the characteristics of objects supported partially or fully by DM annihilation are similarly DM mass-independent.

To understand the differences between hydrogen and DM burning, it is enlightening to consider a star supported entirely by DM annihilation, i.e., $L_{\text{DM}} = L_{\text{surf}}$. Using equation (S5) for the radius in (7), we can find an analytic solution when gravitational focusing is neglected:

$$M_0 = 8.58 \times 10^{-7} \times \frac{(1 + \gamma(\psi) + \alpha\psi)^{1.19895}}{\psi^{1.4993\nu}} \\ \times \left(\frac{\rho_{\text{DM}}}{\text{GeV cm}^{-3}} \frac{v_{\text{DM}}}{50 \text{km s}^{-1}} \frac{f_{\text{cap}}}{b_1^{2.857}} \right)^{0.52475}. \quad (8)$$

In contrast to the equivalent formula for hydrogen-supported objects (6), Eq. (8) has no minimum — DM can support structures of arbitrarily small masses. This is because, unlike hydrogen burning, the DM burning rate does not depend on the stellar properties — DM burn-

ing is ever-present. Including gravitational focusing does not alter this conclusion and in fact produces stronger effects. It is included in our numerical studies below.

Fig. 2 shows numerical solutions for general cases where stars are heated by both, hydrogen and dark matter annihilation, i.e. $L_{\text{surf}} = L_{\text{DM}} + L_{\text{HB}}$. Evidently, the low mass solutions are *dark dwarfs*, supported almost entirely by DM annihilation, whereas the high mass solutions are similar to red dwarf stars — they are supported almost entirely by hydrogen burning but have some amount of DM support. In the transition region, both sources of burning are important. We therefore expect that, unlike in the SM, all brown dwarfs will ultimately evolve into dark dwarfs. Whether this happens within the age of the universe depends on the incident DM flux and circular velocity.

Time Evolution and Stability — To study the time evolution that leads to the formation of dark dwarfs, we use the cooling model introduced in [87, 91]. Using the first law of thermodynamics, the equation for the energy of a contracting star is

$$T \frac{dS}{dt} = \varepsilon - \frac{\partial L_{\text{surf}}}{\partial M} \quad (9)$$

where S is the entropy per unit mass and ε is the energy generation rate per unit mass from burning. Integrating this equation, employing the equation of state for molecular hydrogen, and using the EOS and properties of $n = 3/2$ polytropes one finds [84]

$$\frac{d\psi}{dt} = \frac{\bar{\mu}}{1.5\mu_e^{\frac{8}{3}} E_0} M_0^{-7/3} (1 + \gamma(\psi) + \alpha\psi)^2 (L_{\text{burn}} - L_{\text{surf}}), \quad (10)$$

where $E_0 = 6.73857 \times 10^{49}$ erg, L_{burn} is the energy in

burning, and

$$\frac{1}{\bar{\mu}} = \frac{1}{\mu} + \frac{3X_{H^+}(1-X_{H^+})}{2(2-X_{H^+})} \quad (11)$$

with X_{H^+} the mass fraction of ionized hydrogen; $\bar{\mu} = 1.02$ for parameter point D, see the Supplementary Material. In the absence of any burning, equation (10) implies that ψ will decrease from its initial value i.e., that over time $k_B T$ will decrease relative to E_F (see equation (S3)) and the star will be increasingly supported by degeneracy pressure. In the presence of burning, there is a steady-state when the right hand side of equation (10) is zero i.e., when $L_{\text{burn}} = L_{\text{surf}}$. These are the solutions we derived above. We thus expect that any initial configuration will evolve towards this steady-state, reaching it at sufficiently late times.

The stability of steady-state solutions can be determined as follows. Letting ψ_0 be the value of ψ where the steady-state is achieved, we can write $\psi(t) = \psi_0 + \delta\psi(t)$ and Taylor-expand equation (10) to find $\delta\dot{\psi} = f(\psi_0)\delta\psi + \mathcal{O}(\delta\psi^2)$, where $f(\psi_0)$ is the derivative of the right hand side of (10) with respect to ψ and evaluated at ψ_0 . If $f(\psi_0) < 0$ then the equilibrium is stable. The resulting expressions are long and not informative so we do not give them here. They can be found in our accompanying code. Using the same code, we found that dark dwarfs are always stable. This is true for objects supported by a combination of H-burning and DM burning, or objects supported solely by DM burning. In contrast, only the branch of SM stars (solely H-burning) with $\psi > \psi_{\text{min}}$ is stable.

In Fig. 3 we show properties of objects in the presence of DM annihilation as a function of time found by solving Eq. (10). Several differences between SM objects and those with some amount of DM burning are evident. SM brown dwarfs lighter than the MMHB cool continuously, contracting and becoming dimmer. SM objects heavier than the MMHB cool and evolve to red dwarfs where they are supported by H-burning. In contrast, in the presence of DM burning lighter objects cool similarly to brown dwarfs until they reach the steady-state dark dwarf solution with constant core temperature, radius, and brightness. The time to reach the dark dwarf state is shorter for larger ambient DM densities. The MMHB is also DM density dependent.

We found that for typical galactic center DM velocities and $\rho \gtrsim 10^3 \text{ GeV cm}^{-3}$ objects with mass $M \lesssim 0.05 M_{\odot}$ begin to display differences from brown dwarfs (dashed lines) on a timescale shorter than a Hubble time. Objects in lower density environments will not reach the steady-state within the age of the universe and will appear as brown dwarfs for all intents and purposes. Heavier objects will evolve into red dwarfs but given the same mass their properties are different from the SM prediction due to a non-negligible contribution from DM annihilation. At higher DM densities $\sim 10^5 \text{ GeV cm}^{-3}$, even for higher mass objects there is a significant gap between the

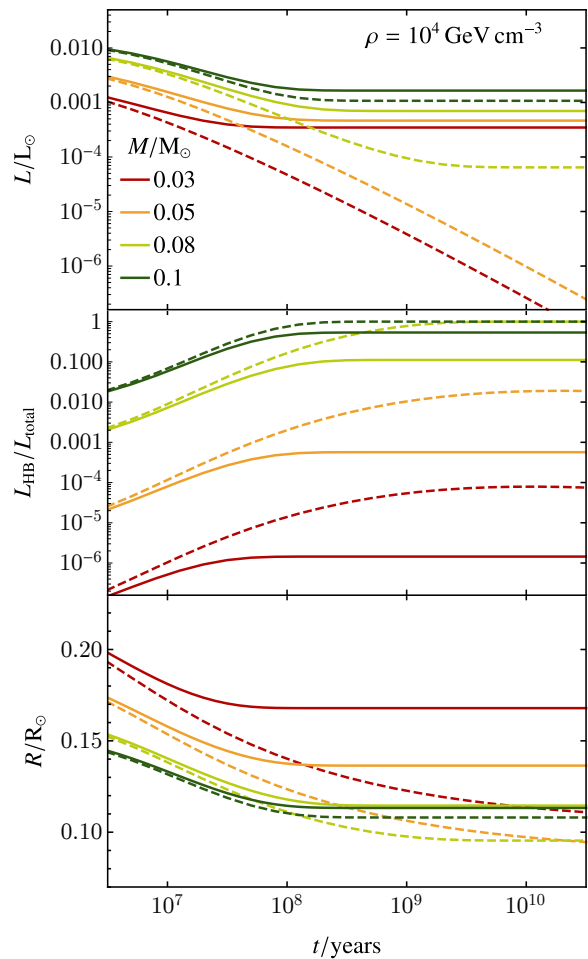


FIG. 3. Time evolution of important stellar properties. The continuous lines correspond to objects evolving in the presence of DM annihilation while dashed lines indicate the SM predictions. Four representative stellar masses indicated in the top panel are shown.

luminosity output of the star and the fraction supplied by hydrogen burning. As we will discuss in the next section, light element burning is also affected leading to a potential search strategy via specific spectroscopic markers.

Lithium burning – The lithium test is a primary method for confirming that an object is a brown dwarf [92]. Observing lithium lines in stellar spectra allows astronomers to trace the core temperature history of young stars and brown dwarfs, distinguishing between different evolutionary epochs. Therefore, deviations from the SM expectation of the lithium-7 abundance may provide a method for detecting dark dwarfs.

Figure 4 shows that for objects close to the stellar mass boundary the core temperatures of DM powered objects is cooler than the SM prediction. The reaction that depletes lithium has a threshold temperature of $\sim 2.5 \times 10^6 \text{ K}$. This suggests that dark dwarfs will have

suppressed lithium burning rates. At lower DM densities, we find a slight increase in core temperature, resulting in a slightly increased depletion rate.

To calculate the surviving light element fraction we consider the relevant reaction in this temperature range



Sub-stellar objects with masses lighter than $0.35M_{\odot}$ are fully convective [93], implying that the ratios of lithium to hydrogen are constant throughout the star. The depletion rate is then given by [94, 95]

$$\frac{d \ln f}{dt} = \frac{4\pi X}{Mm_p} \int_0^R \rho^2 \langle \sigma v \rangle r^2 dr \quad (13)$$

where X is the hydrogen mass fraction, m_p is the proton mass, f is the lithium to hydrogen ratio, and σ the relevant cross section, which we take from [96]. We can solve Eq. (13) using our analytic model but, because the nuclear burning rate (12) is highly sensitive to the core temperature, the model needs to be refined to include the corrections from Coulomb pressure in the stellar core. We explain our method for this in Appendix ID.

In Fig. 5 we show the resulting survival fraction after 1 Gyr. In the case of the SM, we find that Li-7 is depleted in objects heavier than $0.062M_{\odot}$, consistent with other theoretical predictions [97–100]. In contrast, a significant fraction of lithium-7 survives in dark dwarfs of this mass and heavier in regions where $\rho_{\text{DM}} \gtrsim 10^5 \text{ GeV/cm}^3$. Therefore, given an observed mass and estimated age, the spectroscopic detection of lithium can serve as a marker for DM heating.

Conclusion – We have found that the structure, evolution, and fate of sub-stellar objects in the presence of dark matter annihilation is markedly different than the Standard Model predictions. Objects lighter than the hydrogen burning limit begin their lives as brown dwarfs but

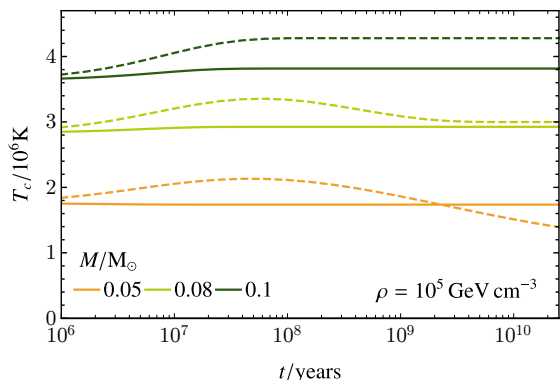


FIG. 4. Time evolution of the core temperatures of five objects with different masses with (solid lines) and without (dashed lines) DM energy injection. Coulomb corrections to the pressure have included.

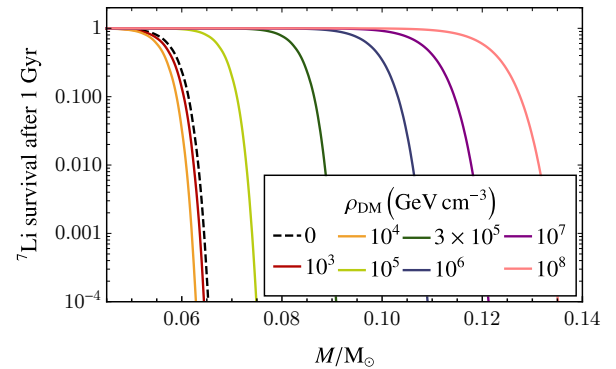


FIG. 5. Lithium survival as a function of mass for different DM densities.

ultimately evolve to become *dark dwarfs* — eternal objects powered by DM burning. Their radii, temperatures, and luminosity are constant. The H-burning limit itself is modified, depending on the incident DM flux. Stars heavier than this behave similarly to red dwarfs but are predicted to be larger and brighter than SM red dwarfs of identical mass due to the additional contribution from DM heating. Their core temperatures can be reduced, causing them to retain lithium in mass ranges where the SM predicts it is depleted. The detection of lithium-7 in objects heavier than the lithium burning limit would provide evidence for the existence of DM heating. The optimum location to search for these signatures is towards the galactic center, where low DM velocities and large densities maximize the incoming DM flux.

SOFTWARE

Mathematica version 12.0.0. All of our results can be reproduced using our code, which is available at the following URL: <https://zenodo.org/records/13141908>.

ACKNOWLEDGEMENTS

DC is supported by the STFC under Grant No. ST/T001011/1. This material is based upon work supported by the National Science Foundation under Grant No. 2207880.

**Dark Dwarfs:
Dark Matter-Powered Sub-Stellar Objects Awaiting Discovery at the Galactic Center**
Supplemental Material

Djuna Croon, Jeremy Sakstein, Juri Smirnov, Jack Streeter

I. ANALYTIC MODEL

In this section we review the derivation of the analytic model that we adopted for our calculations above, explore the effects of the assumptions we have made, and derive the range of validity of our model.

A. Polytrope Model for the Interior

We begin by reviewing the polytropic description of sub-stellar objects, following reference [84]. The EOS for the combination of electron degeneracy pressure P_{deg} and the gas pressure of the ions P_{ion} is an $n = 3/2$ polytrope:

$$P = K\rho^{\frac{5}{3}} \text{ with } K = C\mu_e^{-5/3}(1 + \gamma(\psi) + \alpha\psi). \quad (\text{S1})$$

In the above, $\mu_e = (X + Y/2)^{-1}$ is the number of electrons per baryon (with X and Y the mass fractions of hydrogen and helium respectively); $\alpha = 5\mu_e/2\mu$ with $\mu = ((1+x_H)X + Y/4)$ the mean molecular weight of the ionized hydrogen and helium mixture (x_H is the fraction of ionized hydrogen);

$$C = \frac{2}{5}aA^{\frac{5}{2}}, \quad A = \frac{(3\pi^2\hbar^3N_A)^{\frac{2}{3}}}{2m_e}, \quad a = \frac{2}{3}\frac{4\pi m_e^{\frac{3}{2}}}{(2\pi\hbar)^3}; \quad (\text{S2})$$

and the *degeneracy parameter*

$$\psi = \frac{k_B T}{E_F} \quad (\text{S3})$$

with E_F the Fermi energy. Numerically, $C = 10^{13} \text{ cm}^4 \text{ g}^{-2/3} \text{ s}^{-2}$. The benchmark model in this work fixed $\mu_e = 1.143$, and $\mu = 1.23$ corresponding to a neutral mixture of 75% hydrogen and 25% helium; this gives $\alpha = 2.32$. The function $\gamma(\psi)$ is given by

$$\gamma(\psi) = -\frac{5}{16}\psi \ln(1 + e^{-\frac{1}{\psi}}) + \frac{15}{8}\psi^2 \left[\frac{\pi^2}{3} + \text{Li}_2(-e^{-\frac{1}{\psi}}) \right] \quad (\text{S4})$$

with Li_2 the polylogarithm of order-2. Using the properties of $n = 3/2$ polytropes, it is possible to find expressions for the radius, central temperature, central pressure, and central density as a function of the degeneracy parameter ψ [84]:

$$R = R_0\mu_e^{-5/3}(1 + \gamma(\psi) + \alpha\psi)M_0^{-\frac{1}{3}}, \quad (\text{S5})$$

$$T_c = T_0 M_0^{\frac{4}{3}} \mu_e^{\frac{8}{3}} \frac{\psi}{(1 + \gamma(\psi) + \alpha\psi)^2}, \quad (\text{S6})$$

$$\rho_c = \rho_0 M_0^2 \frac{\mu_e^5}{(1 + \gamma(\psi) + \alpha\psi)^3}, \quad (\text{S7})$$

$$P_c = P_0 M_0^{\frac{10}{3}} \frac{\mu_e^{\frac{20}{3}}}{(1 + \gamma(\psi) + \alpha\psi)^4}, \quad (\text{S8})$$

where $M_0 = M/M_\odot$, $R_0 = 2.80858 \times 10^9 \text{ cm}$, $\rho_0 = 1.28412 \times 10^5 \text{ g/cm}^3$, $T_0 = 7.68097 \times 10^8 \text{ K}$, and $P_0 = 3.26763 \times 10^{12} \text{ g/cm/s}^2$. To make further progress, a model for the photosphere must be specified.

B. Photosphere Models

Model	b_1	ν	$2X_{H+}$
A	2.87	1.58	0.48
B	2.70	1.59	0.50
C	2.26	1.59	0.50
D	2.00	1.60	0.51
E	1.68	1.61	0.52
F	1.29	1.59	0.50
G	0.60	1.44	0.33
H	0.40	1.30	0.18

TABLE S1. Parameter points for the phase transition [101]. Note that points G and H are very close to the second critical point of hydrogen, where a liquid-liquid phase transition occurs.

The photosphere, which defines the effective temperature and the stellar luminosity, is the point at which the optical depth τ falls to $2/3$. At this point, there is a phase transition from the mixture of degenerate electrons and ionic gas described above to a phase of molecular hydrogen. Modeling the latter, one can derive expressions for the effective temperature and luminosity. Several parameter points given in table S1 span the possible range of surface temperatures at which the phase transition takes place:

$$T_{\text{eff}} = b_1 \times 10^6 \rho_e^{2/5} \psi^\nu \text{K}, \quad (\text{S9})$$

where b_1 and ν are parameters of the model [101]. Solving the condition $\tau = 2/3$ yields an expression for the pressure at the photosphere, which can be used to find the density and effective temperature from the ideal gas law (see [84] for the details – here we generalise the solution presented in this work). The result is:

$$T_{\text{eff}} = 1.57466 \times 10^4 b_1 \psi^\nu \left(\frac{M_0^{5/3} \psi^{-\nu}}{b_1 \kappa_R (1 + \gamma + \alpha \psi)^2} \right)^{2/7} \text{K}, \quad (\text{S10})$$

where κ_R is the Rosseland mean opacity. Using the Stefan-Boltzmann law yields the surface luminosity,

$$\frac{L_{\text{surf}}}{L_\odot} = \frac{0.0578353 b_1^3 M_0}{\kappa_R} \psi^{3\nu} \left(\frac{M_0^{5/3} \psi^{-\nu}}{b_1 \kappa_R (1 + \gamma + \alpha \psi)^2} \right)^{1/7}. \quad (\text{S11})$$

This equation is starting point for our work above.

C. Sensitivity to the Molecular Hydrogen Phase Transition

Our calculation relies upon a choice of parameter point for the phase transition, which introduces a source of theoretical uncertainty into our calculations. We explore this in this section. A convenient measure for quantifying the model-dependency is the minimum mass for hydrogen burning, which is DM density and velocity dependent. Since DM annihilation reduces the core temperature and density below the threshold for PP-burning, the MMHB is increased whenever DM burning is important. Demanding $L_{\text{HB}} = L_{\text{DM}}$ leads to the minimum mass shown in figure S1 for the different parameter points given in table S1. The figure demonstrates that the model's predictions only significantly diverge for very large DM densities (with the exception of edge cases G and H), implying that the choice of parameter point is not an important source of uncertainty for our conclusions.

D. Coulomb Corrections to the Equation of State

At low temperatures, the effects of Coulomb repulsion becomes important and the EOS deviates from an $n = 3/2$ polytrope. This has two consequences for our work. First, it limits the applicability of the analytic model we have

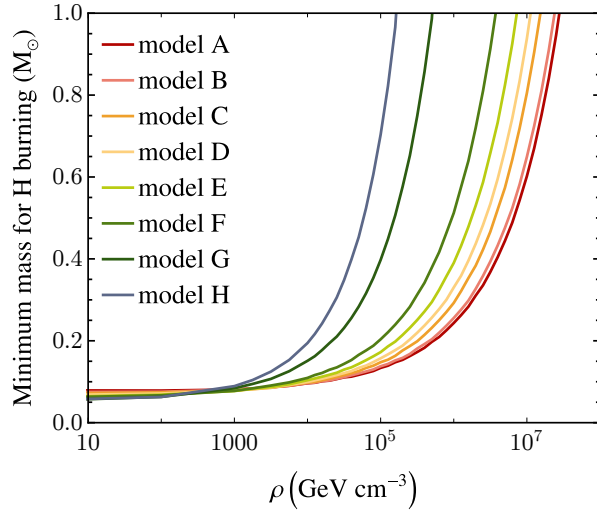


FIG. S1. Minimum mass for hydrogen burning (using the criterion $L_{\text{DM}} = L_{\text{HB}}$) as a function of DM ambient density for different models of the photosphere. Here we use $v_{\text{DM}} = 50 \text{ km/s}$.

assumed to high mass objects and, second, the exponential sensitivity of the lithium-7 burning rate in Eq. (13) mandates that we include these corrections to calculate the core temperature accurately. We derive the mass range where our results are valid and expressions for the corrected core temperature in this section.

The effects of Coulomb interactions depend upon the plasma parameter [85]

$$\Gamma = \frac{e^2}{k_B T} \left(\frac{4\pi\rho}{3m_p} \right)^{\frac{1}{3}}, \quad (\text{S12})$$

where e is the electron charge and m_p is the proton mass. Early in the star's evolution when lithium is being depleted the plasma parameter $\Gamma \ll 1$, corresponding to the Debye-Hückel regime [95]. In this limit, each ion can be thought of as being surrounded by a spherically symmetric but inhomogeneously charged cloud that screens its charge. The Coulomb pressure of these screened charges is [92]

$$P_C = -\frac{e^2}{3} \left(\frac{\pi}{k_B T} \right)^{\frac{1}{2}} \left(\frac{\rho\zeta}{m_p} \right)^{\frac{3}{2}}; \text{ with } \zeta = \sum_j \frac{X_j}{A_j} Z_j (1 + Z_j), \quad (\text{S13})$$

where j runs over all ions with mass fraction X_j , atomic number A_j and charge Z_j . $\zeta = 1.875$ for our benchmark model. The ratio of the Coulomb pressure to the central pressure calculated using the polytrope model for various DM densities is shown in figure S2. In the SM, the polytropic approximation ceases to be valid ($|P_C| > P_c$) when $M < 0.18 M_\odot$. This threshold is reduced when DM annihilation is present. The results we presented in this work correspond to heavier objects.

To incorporate the effects of the Coulomb pressure into our lithium calculation, we use that fact that $T_c \propto \mu_{\text{eff}}^2$ [94, 95] with $\mu_{\text{eff}} = k_B N_A \rho_c T_c / P_c$. At fixed central density, the negative Coulomb pressure reduces the total pressure from the polytrope model's prediction, which raises the central temperature. To incorporate this effect, we first calculate T_c using the polytropic model and then scale this by a factor of $P_c^2 / (P_c + P_C)^2$ to account for the correction to μ_{eff} .

At late times, when the star has cooled and reached its equilibrium state, either red or dark dwarf, the plasma parameter has evolved to $\Gamma \gg 1$ and the Debye-Hückel approximation does not apply. Instead, the plasma is comprised of a sea of degenerate electrons surrounding a lattice of ions arranged to maximize their separation, minimizing their Coulomb repulsion [85]. In this limit, the Coulomb pressure can be found using the Wigner-Seitz approximation where each ion with atomic number Z sits at the center of a neutral sphere containing Z electrons. The Coulomb

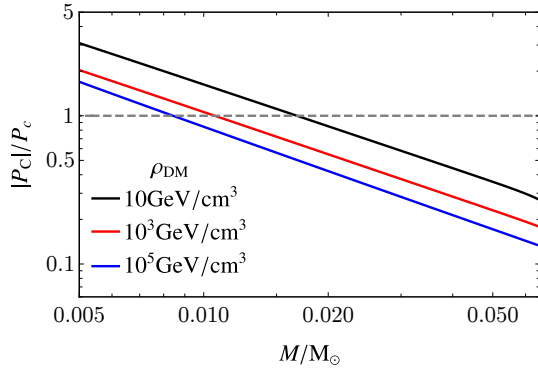


FIG. S2. Ratio of the Coulomb to central pressure as a function of mass for varying DM densities. The polytrope model presented in this work becomes invalid when $|P_C|/P_c > 1$.

pressure is [85]

$$\begin{aligned}
 P_C &= K_C \rho^{\frac{4}{3}}; \\
 K_C &= -\frac{3}{10} \left(\frac{4\pi \langle Z^2 \rangle}{3} \right)^{\frac{1}{3}} e^2 \left(\frac{N_A}{\mu_e} \right)^{\frac{4}{3}} \approx 5.72 \times 10^{12} \text{ g/cm/s}^2.
 \end{aligned} \tag{S14}$$

Comparing the central Coulomb pressure to the central pressure (S8), the latter exceeds the former in objects where $M \lesssim 10^{-3} M_\odot \sim M_{\text{Jupiter}}$, independent of the DM density. Thus, the equilibrium configurations we have studied are valid at even lower masses than estimated above, the caveat being that the polytrope model provides an invalid description of their formation.

[1] G. Steigman and M. S. Turner, Nucl. Phys. B **253**, 375 (1985).

[2] G. Jungman, M. Kamionkowski, and K. Griest, Phys. Rept. **267**, 195 (1996), arXiv:hep-ph/9506380.

[3] G. Bertone, D. Hooper, and J. Silk, Phys. Rept. **405**, 279 (2005), arXiv:hep-ph/0404175 [hep-ph].

[4] G. Bertone and D. Hooper, Rev. Mod. Phys. **90**, 045002 (2018), arXiv:1605.04909 [astro-ph.CO].

[5] A. Geringer-Sameth, S. M. Koushiappas, and M. Walker, Astrophys. J. **801**, 74 (2015), arXiv:1408.0002 [astro-ph.CO].

[6] M. Ackermann *et al.* (Fermi-LAT), Phys. Rev. Lett. **115**, 231301 (2015), arXiv:1503.02641 [astro-ph.HE].

[7] J. Smirnov and J. F. Beacom, Phys. Rev. Lett. **125**, 131301 (2020), arXiv:2002.04038 [hep-ph].

[8] A. Parikh, J. Smirnov, W. L. Xu, and B. Zhou, JHEP **08**, 091 (2023), arXiv:2302.00008 [hep-ph].

[9] B. Batell, M. Pospelov, A. Ritz, and Y. Shang, Phys. Rev. D **81**, 075004 (2010), arXiv:0910.1567 [hep-ph].

[10] M. Pospelov, A. Ritz, and M. B. Voloshin, Phys. Lett. B **662**, 53 (2008), arXiv:0711.4866 [hep-ph].

[11] I. Z. Rothstein, T. Schwetz, and J. Zupan, JCAP **07**, 018 (2009), arXiv:0903.3116 [astro-ph.HE].

[12] M. Pospelov and A. Ritz, Phys. Lett. B **671**, 391 (2009), arXiv:0810.1502 [hep-ph].

[13] F. Chen, J. M. Cline, and A. R. Frey, Phys. Rev. D **80**, 083516 (2009), arXiv:0907.4746 [hep-ph].

[14] P. Schuster, N. Toro, and I. Yavin, Phys. Rev. D **81**, 016002 (2010), arXiv:0910.1602 [hep-ph].

[15] P. Schuster, N. Toro, N. Weiner, and I. Yavin, Phys. Rev. D **82**, 115012 (2010), arXiv:0910.1839 [hep-ph].

[16] N. F. Bell and K. Petraki, Journal of Cosmology and Astroparticle Physics **2011**, 003–003 (2011).

[17] J. L. Feng, J. Smolinsky, and P. Tanedo, Phys. Rev. D **93**, 015014 (2016), [Erratum: Phys. Rev. D **96**, 099901 (2017)], arXiv:1509.07525 [hep-ph].

[18] C. Kouvaris and P. Tinyakov, Phys. Rev. D **82**, 063531 (2010), arXiv:1004.0586 [astro-ph.GA].

[19] J. L. Feng, J. Smolinsky, and P. Tanedo, Phys. Rev. D **93**, 115036 (2016), [Erratum: Phys. Rev. D **96**, 099903 (2017)], arXiv:1602.01465 [hep-ph].

[20] R. Allahverdi, Y. Gao, B. Knockel, and S. Shalgar, Phys. Rev. D **95**, 075001 (2017), arXiv:1612.03110 [hep-ph].

[21] R. K. Leane, K. C. Y. Ng, and J. F. Beacom, Phys. Rev. D **95**, 123016 (2017), arXiv:1703.04629 [astro-ph.HE].

[22] C. Arina, M. Backović, J. Heisig, and M. Lucente, Phys. Rev. D **96**, 063010 (2017), arXiv:1703.08087 [astro-ph.HE].

[23] A. Albert *et al.* (HAWC), Phys. Rev. D **98**, 123012 (2018), arXiv:1808.05624 [hep-ph].

[24] A. Albert *et al.* (HAWC), Phys. Rev. D **98**, 123011 (2018), arXiv:1808.05620 [astro-ph.HE].

[25] M. U. Nisa, J. F. Beacom, S. Y. BenZvi, R. K. Leane, T. Linden, K. C. Y. Ng, A. H. G. Peter, and B. Zhou, (2019), arXiv:1903.06349 [astro-ph.HE].

[26] C. Niblaeus, A. Beniwal, and J. Edsjo, JCAP **11**, 011 (2019), arXiv:1903.11363 [astro-ph.HE].

[27] A. Cuoco, P. De La Torre Luque, F. Gargano, M. Gustafsson, F. Loparco, M. Mazziotta, and D. Serini, Phys. Rev. D **101**, 022002 (2020), arXiv:1912.09373 [astro-ph.HE].

[28] D. Serini, F. Loparco, and M. N. Mazziotta (Fermi-LAT), PoS **ICRC2019**, 544 (2020).

[29] J. F. Acevedo, J. Bramante, A. Goodman, J. Kopp, and T. Opferkuch, JCAP **04**, 026 (2021), arXiv:2012.09176 [hep-ph].

[30] M. Mazziotta, F. Loparco, D. Serini, A. Cuoco, P. De La Torre Luque, F. Gargano, and M. Gustafsson, Phys. Rev. D **102**, 022003 (2020), arXiv:2006.04114 [astro-ph.HE].

[31] N. F. Bell, J. B. Dent, and I. W. Sanderson, (2021), arXiv:2103.16794 [hep-ph].

[32] D. Bose, T. N. Maity, and T. S. Ray, Phys. Rev. D **105**, 123013 (2022), arXiv:2112.08286 [hep-ph].

[33] J. Smirnov, A. Goobar, T. Linden, and E. Mörtzell, Phys. Rev. Lett. **132**, 151401 (2024), arXiv:2211.00013 [astro-ph.CO].

[34] D. Croon and J. Sakstein, Phys. Rev. D **109**, 103021 (2024), arXiv:2310.20044 [astro-ph.HE].

[35] I. John, R. K. Leane, and T. Linden, (2024), arXiv:2405.12267 [astro-ph.HE].

[36] I. Goldman and S. Nussinov, Phys. Rev. D **40**, 3221 (1989).

[37] A. Gould, B. T. Draine, R. W. Romani, and S. Nussinov, Phys. Lett. B **238**, 337 (1990).

[38] C. Kouvaris, Phys. Rev. D **77**, 023006 (2008), arXiv:0708.2362 [astro-ph].

[39] G. Bertone and M. Fairbairn, Phys. Rev. D **77**, 043515 (2008), arXiv:0709.1485 [astro-ph].

[40] A. de Lavallaz and M. Fairbairn, Phys. Rev. D **81**, 123521 (2010), arXiv:1004.0629 [astro-ph.GA].

[41] C. Kouvaris and P. Tinyakov, Phys. Rev. D **82**, 063531 (2010), arXiv:1004.0586 [astro-ph.GA].

[42] S. D. McDermott, H.-B. Yu, and K. M. Zurek, Phys. Rev. D **85**, 023519 (2012), arXiv:1103.5472 [hep-ph].

[43] C. Kouvaris and P. Tinyakov, Phys. Rev. Lett. **107**, 091301 (2011), arXiv:1104.0382 [astro-ph.CO].

[44] T. Guver, A. E. Erkoca, M. Hall Reno, and I. Sarcevic, JCAP **1405**, 013 (2014), arXiv:1201.2400 [hep-ph].

[45] J. Bramante, K. Fukushima, and J. Kumar, Phys. Rev. D **87**, 055012 (2013), arXiv:1301.0036 [hep-ph].

[46] N. F. Bell, A. Melatos, and K. Petraki, Phys. Rev. D **87**, 123507 (2013), arXiv:1301.6811 [hep-ph].

[47] J. Bramante, K. Fukushima, J. Kumar, and E. Stopnitzky, Phys. Rev. D **89**, 015010 (2014), arXiv:1310.3509 [hep-ph].

[48] B. Bertoni, A. E. Nelson, and S. Reddy, Phys. Rev. D **88**, 123505 (2013), arXiv:1309.1721 [hep-ph].

[49] C. Kouvaris and P. Tinyakov, Phys. Rev. D **83**, 083512 (2011), arXiv:1012.2039 [astro-ph.HE].

[50] M. McCullough and M. Fairbairn, Phys. Rev. D **81**, 083520 (2010), arXiv:1001.2737 [hep-ph].

[51] M. Angeles Perez-Garcia and J. Silk, Phys. Lett. B **744**, 13 (2015), arXiv:1403.6111 [astro-ph.SR].

[52] J. Bramante, Phys. Rev. Lett. **115**, 141301 (2015), arXiv:1505.07464 [hep-ph].

[53] P. W. Graham, S. Rajendran, and J. Varela, Phys. Rev. D **92**, 063007 (2015), arXiv:1505.04444 [hep-ph].

[54] M. Cermenno, M. Perez-Garcia, and J. Silk, Phys. Rev. D **94**, 063001 (2016), arXiv:1607.06815 [astro-ph.HE].

[55] P. W. Graham, R. Janish, V. Narayan, S. Rajendran, and P. Riggins, Phys. Rev. D **98**, 115027 (2018), arXiv:1805.07381 [hep-ph].

[56] J. F. Acevedo and J. Bramante, Phys. Rev. **D100**, 043020 (2019), arXiv:1904.11993 [hep-ph].

[57] R. Janish, V. Narayan, and P. Riggins, Phys. Rev. **D100**, 035008 (2019), arXiv:1905.00395 [hep-ph].

[58] R. Krall and M. Reece, Chin. Phys. **C42**, 043105 (2018), arXiv:1705.04843 [hep-ph].

[59] D. McKeen, A. E. Nelson, S. Reddy, and D. Zhou, Phys. Rev. Lett. **121**, 061802 (2018), arXiv:1802.08244 [hep-ph].

[60] M. Baryakhtar, J. Bramante, S. W. Li, T. Linden, and N. Raj, Phys. Rev. Lett. **119**, 131801 (2017), arXiv:1704.01577 [hep-ph].

[61] N. Raj, P. Tanedo, and H.-B. Yu, Phys. Rev. **D97**, 043006 (2018), arXiv:1707.09442 [hep-ph].

[62] N. F. Bell, G. Busoni, and S. Robles, JCAP **1809**, 018 (2018), arXiv:1807.02840 [hep-ph].

[63] C.-S. Chen and Y.-H. Lin, JHEP **08**, 069 (2018), arXiv:1804.03409 [hep-ph].

[64] R. Garani, Y. Genolini, and T. Hambye, JCAP **05**, 035 (2019), arXiv:1812.08773 [hep-ph].

[65] B. Dasgupta, A. Gupta, and A. Ray, JCAP **08**, 018 (2019), arXiv:1906.04204 [hep-ph].

[66] K. Hamaguchi, N. Nagata, and K. Yanagi, Phys. Lett. **B795**, 484 (2019), arXiv:1905.02991 [hep-ph].

[67] D. A. Camargo, F. S. Queiroz, and R. Sturani, JCAP **1909**, 051 (2019), arXiv:1901.05474 [hep-ph].

[68] N. F. Bell, G. Busoni, and S. Robles, JCAP **1906**, 054 (2019), arXiv:1904.09803 [hep-ph].

[69] J. F. Acevedo, J. Bramante, R. K. Leane, and N. Raj, JCAP **03**, 038 (2020), arXiv:1911.06334 [hep-ph].

[70] A. Joglekar, N. Raj, P. Tanedo, and H.-B. Yu, (2019), arXiv:1911.13293 [hep-ph].

[71] A. Joglekar, N. Raj, P. Tanedo, and H.-B. Yu, (2020), arXiv:2004.09539 [hep-ph].

[72] N. F. Bell, G. Busoni, S. Robles, and M. Virgato, (2020), arXiv:2004.14888 [hep-ph].

[73] R. Garani, A. Gupta, and N. Raj, (2020), arXiv:2009.10728 [hep-ph].

[74] R. K. Leane, T. Linden, P. Mukhopadhyay, and N. Toro, Phys. Rev. D **103**, 075030 (2021), arXiv:2101.12213 [astro-ph.HE].

[75] D. Bose, T. N. Maity, and T. S. Ray, JCAP **05**, 001 (2022), arXiv:2108.12420 [hep-ph].

[76] M. Collier, D. Croon, and R. K. Leane, Phys. Rev. D **106**, 123027 (2022), arXiv:2205.15337 [gr-qc].

[77] G. D. Mack, J. F. Beacom, and G. Bertone, Phys. Rev. D **76**, 043523 (2007), arXiv:0705.4298 [astro-ph].

[78] J. Bramante, A. Buchanan, A. Goodman, and E. Lodhi, Phys. Rev. D **101**, 043001 (2020), arXiv:1909.11683 [hep-ph].

[79] R. K. Leane and T. Linden, (2021), arXiv:2104.02068 [astro-ph.HE].

[80] D. Croon and J. Smirnov, (2023), arXiv:2309.02495 [hep-ph].

[81] R. K. Leane and J. Smirnov, Phys. Rev. Lett. **126**, 161101 (2021), arXiv:2010.00015 [hep-ph].

[82] J. Sakstein, Phys. Rev. Lett. **115**, 201101 (2015), arXiv:1510.05964 [astro-ph.CO].

[83] J. Sakstein, Phys. Rev. D **92**, 124045 (2015), arXiv:1511.01685 [astro-ph.CO].

[84] S. Auddy, S. Basu, and S. R. Valluri, Advances in Astronomy **2016**, 574327 (2016), arXiv:1607.04338 [astro-ph.SR].

[85] D. D. Clayton, *Principles of stellar evolution and nucleosynthesis* (1983).

[86] D. Saumon, W. B. Hubbard, A. Burrows, T. Guillot, J. I. Lunine, and G. Chabrier, Astrophys. J. **460**, 993 (1996), arXiv:astro-ph/9510046.

[87] A. Burrows and J. Liebert, Reviews of Modern Physics **65**, 301 (1993).

[88] B. Freytag, F. Allard, H.-G. Ludwig, D. Homeier, and M. Steffen, Astron. Astrophys. **513**, A19 (2010), arXiv:1002.3437 [astro-ph.SR].

[89] R. K. Leane and J. Smirnov, (2023), arXiv:2309.00669 [hep-ph].

[90] E. V. Karukes, M. Benito, F. Iocco, R. Trotta, and A. Geringer-Sameth, JCAP **05**, 033 (2020), arXiv:1912.04296 [astro-ph.GA].

[91] D. J. Stevenson, IN: Annual review of astronomy and astrophysics. Vol. 29 (A92-18081 05-90). Palo Alto, CA, Annual Reviews, Inc., 1991, p. 163-193. **29**, 163 (1991).

[92] R. Rebolo, E. L. Martin, and A. Magazzu, ApJ **389**, L83 (1992).

[93] G. Chabrier and I. Baraffe, Astron. Astrophys. **327**, 1039 (1997), arXiv:astro-ph/9704118.

[94] L. Bildsten, E. F. Brown, C. D. Matzner, and G. Ushomirsky, Astrophys. J. **482**, 442 (1997), arXiv:astro-ph/9612155.

[95] G. Ushomirsky, C. D. Matzner, E. F. Brown, L. Bildsten, V. G. Hilliard, and P. C. Schroeder, Astrophys. J. **497**, 253 (1998), arXiv:astro-ph/9711099.

[96] G. R. Caughlan and W. A. Fowler, Atomic Data and Nuclear Data Tables **40**, 283 (1988).

[97] F. Pozio, Mem. Soc. Astron. Italiana **62**, 171 (1991).

[98] L. A. Nelson, S. Rappaport, and E. Chiang, ApJ **413**, 364 (1993).

[99] G. Chabrier, I. Baraffe, and B. Plez, ApJ **459**, L91 (1996).

[100] M. W. Phillips, P. Tremblin, I. Baraffe, G. Chabrier, N. F. Allard, F. Spiegelman, J. M. Goyal, B. Drummond, and E. Hébrard, A&A **637**, A38 (2020), arXiv:2003.13717 [astro-ph.SR].

[101] G. Chabrier, D. Saumon, W. B. Hubbard, and J. I. Lunine, Astrophysical Journal, Part 1 (ISSN 0004-637X), vol. 391, no. 2, June 1, 1992, p. 817-826. **391**, 817 (1992).